Modeling multi-fraction coastal aeolian sediment transport with horizontal and vertical grain size variability

C.O. van IJzendoorn[a], C. Hallin[a, b], A.J.H.M. Reniers[a], S. de Vries[a]

a) Department of Hydraulic Engineering, Delft University of Technology, Delft, the Netherlands

b) Lund University

Key points

- The effect of multi-fraction transport and spatial grain size variations were examined with the numerical aeolian transport model AeoLiS.
- The D_{50} can be used as a representative grain size in aeolian sediment transport modeling on a time scale of days to years.
- The bed surface grain size in the upwind, source area might be the most relevant to include in aeolian sediment transport models.

Abstract

Grain size affects the rates of aeolian sediment transport on beaches. Sediment in coastal environments typically consists of multiple grain size fractions and exhibits spatiotemporal variations. Still, conceptual and numerical aeolian transport models are simplified and often only include a single fraction that is constant over the model domain. It is unclear to what extent this simplification is valid and if the inclusion of multi-fraction transport and spatial grain size variations affects aeolian sediment transport simulations and predictions of coastal dune development. This study applies the numerical aeolian sediment transport model AeoLiS to compare single-fraction to multi-fraction approaches for a range of grain size distributions and spatial grain size scenarios. The results show that on timescales of days to years, single-fraction simulations with the median grain size, D_{50}, often give similar results to multi-fraction simulations provided the wind is able to mobilize all fractions within that time frame. On these timescales, vertical variability in grain size has a limited effect on total transport rates, but it does influence the simulation results on minute timescales. Horizontal grain size variability influences both the total transport rates and the downwind bed grain size composition. The results provide new insights into the influence of beach sediment composition and spatial variability on total transport rates towards the dunes. The findings of this study can guide the implementation of grain size variability in numerical aeolian sediment transport models.

Plain language summary

The growth of coastal dunes is caused by the wind, which moves sand from the beach to the dunes. The sand grains on the beach have different sizes. For instance, the size of the sand grains can vary from the waterline to the start of the dunes. Small sand grains are more easily picked up by the wind than larger, heavier grains. Thus, the size of sand grains and how they are spread over the beach can impact how much sand is moved by the wind. We use computer simulations to calculate how much sand is moved by the wind during different conditions. We investigate how different assumptions about the grain size on the beach influence these calculations. The results show that the calculations with one single sand size, in most cases, give comparable results to simulations with more complicated sand size variations. The simplified approach is beneficial because it reduces the need for detailed field data of grain sizes for future calculations.

Index terms and keywords

4217 Coastal processes

4546 Nearshore processes

4558 Sediment transport

0545 Modeling

Key words: grain size, aeolian processes, AeoLiS, beaches

1. Introduction

Sediment available for aeolian transport in coastal settings is characterized by a grain size distribution that is typically described with a range of grain size fractions (Krumbein, 1934). Grain size affects aeolian sediment transport due to the larger drag and lift force that is necessary to displace coarser grains (Durán et al., 2011; Sarre, 1987). Grain size also alters the creep and saltation trajectory of sediment (e.g., Cheng et al., 2015; Zhang et al., 2021). Therefore, different grain size fractions lead to different rates of sediment transport.

Field measurements on beaches have shown considerable spatial variations in grain size in the alongshore (Hallin, et al., 2019a), cross-shore (Bauer, 1991; Çelikoğlu et al., 2006; Edwards, 2001; Sonu, 1972; Stauble & Cialone, 1997; van der Wal, 2000a; van IJzendoorn et al., 2022) and vertical dimension (van IJzendoorn et al., 2022). These horizontal and vertical grain size variations are expected to have a

complex, combined effect on aeolian sediment transport, especially since grain size and sediment transport continuously interact. However, it is unknown how the spatial grain size variability influences the rate of aeolian transport towards the dunes.

Despite the variable transport rates for the different grain size fractions available in beach sediment, aeolian models (e.g., Hoonhout and de Vries, 2016; van Dijk et al., 1999; Roelvink and Costas, 2019, Hallin, et al., 2019c) are typically simplified by using a single fraction throughout the model domain (e.g., Hallin, et al., 2019b; Hoonhout & de Vries, 2016; van der Wal, 2000b). However, some models can simulate multi-fraction transport, including the effect of sorting and the associated changes to the grain size distribution in the bed. An example of such a model is AeoLis, a process-based aeolian sediment transport model. The model has been used for multi-fraction simulations (e.g. Hoonhout & de Vries, 2016, 2019) but the difference in transport rates compared to single-fraction simulations has not yet been fully quantified.

We hypothesize that the inclusion of multi-fraction transport and spatial grain size variations in aeolian transport simulations has a considerable effect on the calculated sediment transport. Investigating these effects in an aeolian sediment transport model can provide new insights into the functioning of the aeolian sediment transport chain. Additionally, quantifying the effects of grain size is expected to provide important recommendations for grain size as an input parameter in future aeolian transport modeling that is used for coastal dune development predictions. This quantification can also impact the use of grain size as a design parameter in the implementation of interventions in the coastal dune system (e.g., Kroon et al., 2022).

This research investigates to what extent sorting in multi-fraction sediment transport modeling and spatial grain size variations impact aeolian sediment transport. The important processes in the aeolian sediment transport chain are discussed in Section 2.1. The choice for a numerical model as study tool is explained in Section 2.2. The numerical implementation of different grain size scenarios that were simulated are presented in Section 3. In Section 4, the aeolian transport rates that resulted from the different grain size scenarios are presented. These results are discussed in Section 5 and the conclusions are drawn in Section 6.

2. Background

2.1. Modeling the aeolian sediment transport chain

Model concepts of the impact of multi-fraction transport and spatial grain size variations require that all relevant aeolian sediment transport processes are represented in the model (Figure 1). The bed stratigraphy consists of vertical layering with varying grain size distributions (van IJzendoorn et al. 2022). The wind forcing, the horizontal influx (upwind) and outflux (downwind) of sediment, and the sediment available at the bed surface determine the rate of deposition/erosion that occurs (de Vries, et al., 2014a; Houser, 2009). High wind scenarios increase the probability of erosion, however, coarse sediment at the surface can impede pickup of sediment when armoring occurs (Gao et al., 2016; McKenna Neuman & Bédard, 2017).

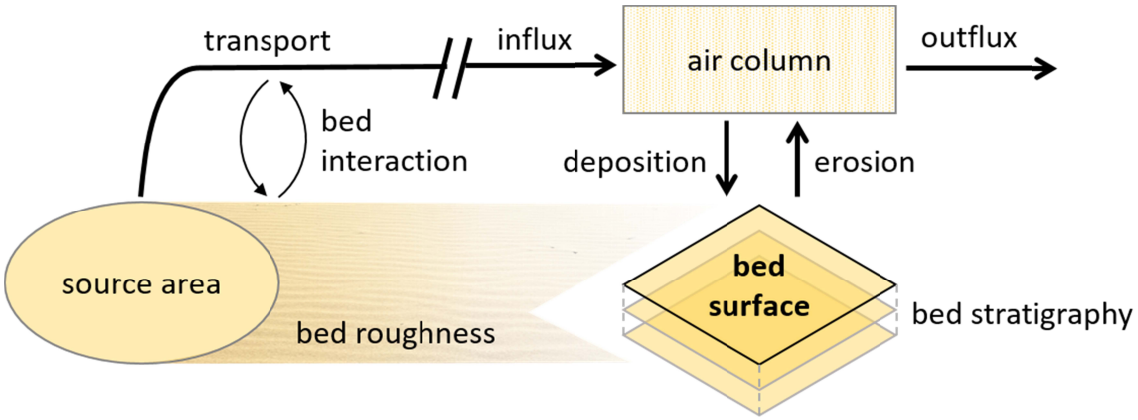

Figure 1 – Conceptual representation of the interaction between grain size on the bed surface and in the air column during aeolian sediment transport on the beach.

Additionally, bed roughness and the fetch effect may impact whether erosion or deposition takes place. A larger bed roughness increases the transport capacity (Bagnold, 1937b). Bed roughness can vary greatly on the beach as the bed characteristics are variable and dynamic (Bristow et al., 2022; Field & Pelletier, 2018; Owen, 1964; Sherman, 1992; van Rijn & Strypsteen, 2020). The fetch effect describes how the sediment concentration in the air column increases downwind from the start of the domain until fully developed transport is reached (Bauer & Davidson-Arnott, 2002; Delgado-Fernandez, 2010; Gillette et al., 1996). Fully developed transport occurs when there is no additional pickup of sediment anymore and the influx and outflux at a certain location are equal. Erosion and deposition of sediment results from the difference between actual and equilibrium transport.

In case of erosion, the change in bed surface grain size will be dominated by the bed stratigraphy, especially as underlying sediment layers can be exposed and armor layers can form (Hoonhout and de Vries, 2016). In the case of deposition, the change in bed surface grain size will be dominated by the grain size of the sediment in the air column. The sediment composition in the air column is determined

by processes that occur upwind of the bed surface location. The sediment in the air column was picked up from the source area during antecedent wind conditions and was transported towards the bed surface location (i.e. advection). During this transport, bed interaction (i.e. the splash process) might have resulted in an exchange of sediment between the air and the bed (Anderson & Haff, 1988). This exchange can alter the grain size distribution of the sediment in the air column depending on the sediment composition of the beach between the source area and the bed surface location (Dong et al., 2004).

2.2. Studying the role of grain size in the sediment transport chain

In the field, it is difficult to distinguish the effect of grain size variability from other varying environmental conditions, such as the wind field, bedforms, and surface moisture. Field measurements are often limited to a single location, which means they can show temporal patterns in grain size composition that are related to transport processes occurring upwind (Cohn et al., 2022; Field & Pelletier, 2018). Furthermore, it is difficult to observe the vertical bed composition at a relevant scale with non-invasive observation techniques (van IJzendoorn et al., 2022). Here, modeling has a major advantage as it allows the recording and investigation of the transport chain, including the source area, advective transport through the air, and bed surface grain size throughout the domain.

The numerical aeolian sediment transport model AeoLiS was selected as a tool to simulate the effect of grain size on aeolian transport in this research. AeoLiS provides a systematic approach to studying spatiotemporal grain size variations. Distinguishing the impact of grain size from the many other factors that affect aeolian sediment transport on the beach is challenging. Therefore, wind tunnel experiments, in which the environmental conditions can be controlled, have been used to isolate individual aspects of aeolian sediment transport (e.g., grain size by Bagnold, 1937a, and shells by McKenna Neuman et al., 2012). However, it would be difficult if not impossible to set up experiments with complex bed composition variations at reasonable monetary, time, and labor costs. Numerical modeling provides an opportunity to gain useful insights into this type of variations at relatively low cost.

3. Methods

3.1. Model description

The multi-fraction approach of the AeoLiS model makes it suitable to study the effect of grain size variations on aeolian transport. The sediment bed in the model consists of a user-defined number of vertical layers and horizontal grid cells. The definition of vertical layers is crucial for describing the

process of coarsening and fining and its associated vertical grain size gradients in the model. The bed composition, which is the initial spatial grain size variation of the bed throughout the domain, can be prescribed in the latest version of the model (AeoLiS v2.1.0 by AeoLiS Development Team, 2022). Transport, erosion and deposition are calculated for each grain size fraction individually (Figure 2), allowing for surface armoring to occur as finer grains are removed, and coarse grains stay behind (Hoonhout & de Vries, 2016).

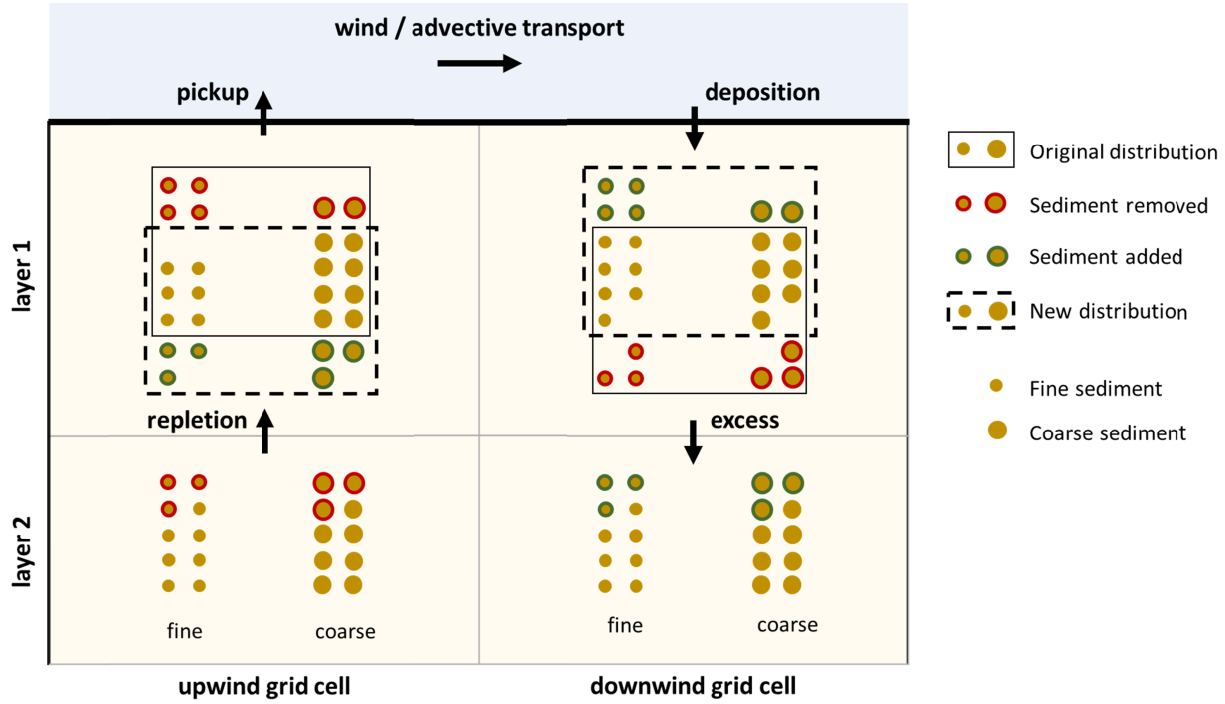

Figure 2 – Schematization of the implementation of discrete layering in AeoLiS and the effects of erosion and deposition on the grain size distribution. The total mass in each grid cell of each layer is normalized. This normalization is represented by the fact that the grain size distribution in each grid cell (indicated by solid and dashed, black rectangles) should contain exactly 20 sediment grains. In the upwind grid cell, the bed surface layer shows coarsening due to differential erosion of the sediment fractions. In the downwind grid cell, the bed surface layer shows fining because the deposited sediment is a reflection of the predominantly fine sediment available in the air column. The movement of repletion sediment in the upwind grid cell is dependent on the grain size distribution in layer 2, whereas the movement of excess sediment in the downwind grain cell is dependent on the original distribution in layer 1. Adapted from Hoonhout & Vries (2016).

In AeoLiS, the equilibrium transport rate for each grain size fraction is calculated based on an adapted version of the Bagnold equation (Bagnold, 1937b), formulated as

$$Q = C\frac{\rho_a}{g}\left(u_* - u_{t,*}\right)^3 \quad (1)$$

in which Q (kg/m/s) is the aeolian sediment transport rate in the case of saturated transport, where C (-) is a constant equal to 1.5 that accounts for sediment gradation, ρ_a (kg/m3) is the density of air, and g (m/s2) is the gravitational constant. The u_* is the surface shear velocity which represents the force exerted on the surface by the wind. The $u_{t,*}$ is the threshold shear velocity which represents the shear velocity at which grains at the surface start to move (initiation of motion).

The threshold shear velocity is expressed as

$$u_{t,*} = A\sqrt{\frac{\rho_s - \rho_a}{\rho_a} g\, d} \quad (2)$$

in which ρ_s (kg/m3) is the density of the sediment, d is the grain size diameter, and A is a constant coefficient equal to 0.085. The shear velocity is expressed as

$$u_* = u_w \frac{\kappa}{\ln\frac{z}{z_0}} \quad (3)$$

in which u_w (m/s) is the wind velocity at height z (m) and z_0 (m) is the aerodynamic roughness. The κ (-) represents the Von Karman constant. The z_0 depends on the surface characteristics of the bed (i.e., the bed roughness). It should be noted that, in this research, the Nikuradse roughness method was used to calculate the aerodynamic roughness ($z_0 = \frac{d}{30}$), as it allows for spatially varying grain sizes to impact the bed roughness through the median grain size, D_{50}, of the bed surface in each individual grid cell.

The equilibrium transport rate resulting from Equation 1 is used in a 1-D advection scheme (de Vries, et al., 2014b),

$$\frac{\partial c}{\partial t} + u_z \frac{\partial c}{\partial x} = \frac{c_{sat} - c}{T}$$

This equation is applied to calculate the sediment mass per unit area c (kg/m^2) throughout time, indicated as t (s), and space, indicated as x (m). The u_z (m/s) represents the wind velocity at height z (m). The bed exchange, which consists of erosion and deposition, is determined as the difference between the saturated sediment concentration c_{sat} (kg/m^2) and the instantaneous sediment concentration c (i.e., the sediment concentration already present in the air) divided by an adaptation time scale T (usually 1 s). The adaptation time scale results in a simulation of the fetch effect (e.g., Bauer & Davidson-Arnott, 2003; Gillette et al., 1996), where the sediment concentration increases downwind from the start of the

domain. The increase to the maximum sediment concentration (i.e., where the normalized sediment concentration equals 1) requires a longer fetch with larger wind speeds and finer grain sizes as the saturated sediment concentration increases. Additionally, the bed exchange is maximized by the sediment that is available at the bed.

For this study, the AeoLiS model was extended with the capability to input spatially varying bed grain size properties both in the horizontal (cross-shore and longshore) and vertical domains. The source code and documentation are open-source (https://github.com/openearth/aeolis-python). More details on the model concepts in AeoLiS and their numerical implementation can be found in De Vries, et al. (2014b) and Hoonhout & Vries (2016).

The set-up of the model used in this study was based on an idealized beach environment. The 1D domain was 200 m long with a grid size of 1 m. The seaward boundary (x=0 m) had zero influx of aeolian sediment, and the landward boundary was open (x=200 m), so sediment can leave the domain. In the idealized beach environment, the effect of waves and tides was excluded, and only the wind that blows over a flatbed was taken into account. The wind direction was constant, and blowing in the direction of the grid from 0 to 200 m. In all simulations, nearly all default parameters of AeoLiS (v2.1.0) were used (AeoLiS Development Team, 2023). Only the parameters related to different grain size scenarios and time scales (discussed in Section 3.2 and 3.3), and the bed interaction (set to 0.05, following Hoonhout & Vries (2016)) deviated from the default settings.

The idealized beach environment was used to create scenarios with different temporal scales and different spatial grain size variations. To enable the execution of the different scenarios two main input parameters were varied: the wind forcing and the bed composition. The impact of these variations were studied by recording the sediment flux that leaves the domain. The model setup used for all scenarios, and the python code used for the analysis and generation of the figures in this paper are freely available (van IJzendoorn, 2023).

3.2. Grain size scenarios

Several grain size scenarios were tested to investigate the effect of grain size variability: single-fraction, multi-fraction, horizontal variation, and vertical layering. The different grain size scenarios were simulated over different timescales with both static and variable winds to investigate the impact of sorting and wind climate. For all scenarios, a corresponding single-fraction reference grain size was used

to quantify the effect of the scenario on the sediment transport. An overview of the scenarios and the 25 different cases that were formulated is presented in Table 1.

Table 1 – Overview of the different grain size scenarios and their associated cases, including the time scales at which the cases were executed. The underlined time scales are not shown in the Results section because they exhibit behavior comparable to the other time scales.

Scenario	**# of cases**	**Case description**		**Time scale**
Single-fraction	6	125, 250, 300, 375, 500, 1000 and 2000 µm		10 min, 1 day, 1 year
Multi-fraction	1	Two fractions	50%-50%	1 day, <u>1 year</u>
	3		20%-80%	<u>1 day</u>, 1 year
	4		varied percentage	<u>1 day</u>, 1 year
	6	Full particle size distribution		1 day, 1 year
Spatial variations	3	Horizontal		10 min, <u>1 day</u>, 1 year
	2	Vertical		10 min, 1 day, <u>1 year</u>

A single fraction scenario and a multi-fraction scenario, which included cases with two-fraction mixes and full particle size distributions (PSDs), were executed to investigate the effect of including multi-fraction transport in aeolian sediment transport simulations (Figure 3). For the single-fraction scenario, cases were created with one grain size class between 125 and 2000 µm that was the same in the entire bed (Figure 3a). In the two-fraction mix cases, grain size classes between 125 and 2000 µm were used. Two grain size classes were chosen with different weights assigned to both classes for each case (Figure 3b, c and d). The percentages used in the context of grain size distributions indicate weight percentages. The single-fraction reference for the 50-50% and 80-20% mixes was defined as the average grain size. The single-fraction 125 µm case was used as a reference for the varied percentage mix.

For the particle size distribution cases, 6 PSDs were created with Qgrain (Liu et al., 2021). The shape parameters (i.e., mean, standard deviation, weight and skewness) of the average grain size distribution of all samples collected in Noordwijk as presented in van IJzendoorn et al. (2022) were determined by fitting a skewed normal distribution. Subsequently, the median grain size (250 and 500 µm) and standard deviation (σ = 0.32, 0.62 and 0.92) were varied to create 6 PSDs (Figure 3e). The median grain

size of each PSD was used as the reference case. The full particle size distribution was expressed as the mass weight of each grain size class with 20 classes ranging from 50 to 1950 µm.

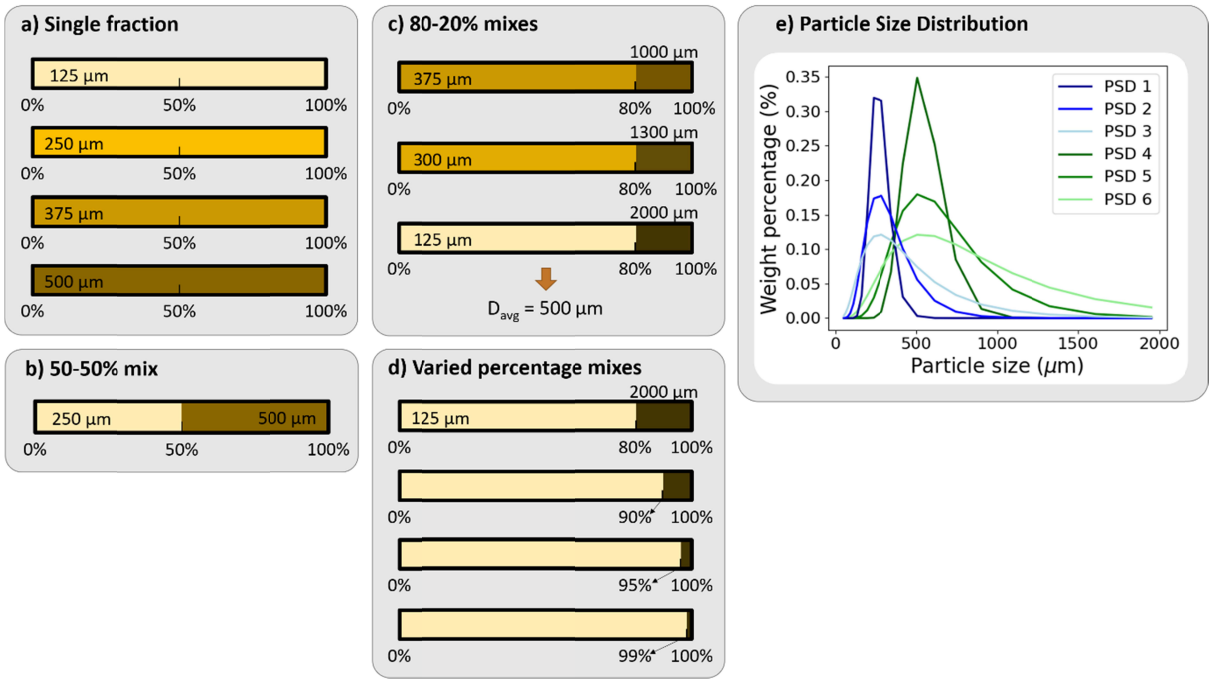

Figure 3 – Overview of the different grain size scenarios that were used in simulations with a spatially invariant grain size. For (c) the 80-20% mixes all had the same average grain size (D_{avg} = 500 µm). In (d) the varied percentage mixes, two fixed grain size classes were used (i.e. 125 and 2000 µm), but the median grain size varied as the mass distribution over two fixed grain size classes was varied. The (e) particle size distribution scenario consisted of 6 different PSDs with a median grain size of approximately 250 (blue) or 500 µm (green) and varying distribution widths.

The effect of spatial grain size variations on aeolian sediment transport simulations was investigated with horizontal variation and vertical layering scenarios (Figure 4). Horizontal variations were implemented with a coarse-fine, fine-coarse and fine-coarse-fine gradient (Figure 4a). To create these gradients, the weight of a fine fraction (250 µm) and a coarse fraction (500 µm) were varied between 0 and 100% along the domain. In all cases, the average distribution of the two fractions was 50-50%, thus, the average grain size of 375 µm was used as a reference case. The different spatial distributions represent fining and coarsening gradients found in the field. Specifically, the gradient with coarse material in the middle represents field situations where the coarsest sediments have been found on the berm. The horizontal spatial gradients were applied to all vertical layers in the domain, including the

lowest one. This results in the initial grain size gradient being continuously supplied from below. This assumes that the initial bed stratigraphy is uniform with depth.

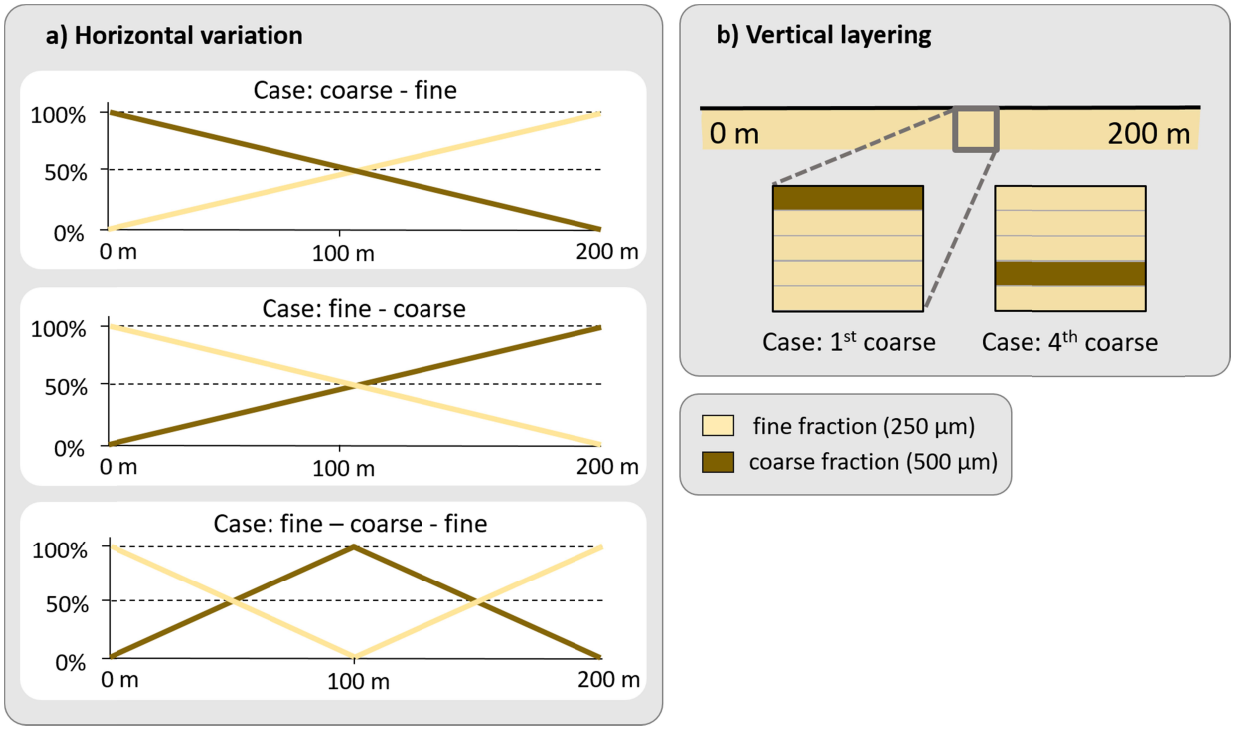

Figure 4 – Overview of the different grain size scenarios that were used in simulations with a spatially varying grain size gradients. (a) The horizontal variation scenario consisted of three different gradients where a fine (250 µm) and coarse (500 µm) grain size class were spatially mixed. (b) In the vertical layering scenario, all layers consisted of the fine grain size class (250 µm) apart from one coarse layer (500 µm).

The effect of grain size variations in the vertical dimension was investigated with a vertical layering scenario. In this scenario, the grain size layering at the beach surface was represented by 5 layers, consisting of either fine (250 µm) or coarse (500 µm) sediment (Figure 4b). In the first case, the upper layer consisted of coarse sediment, whereas in the second case, the fourth layer consisted of coarse sediment. Both cases have an average grain size of 300 µm, so a single-fraction case was executed for comparison with the vertical layering scenario. In both cases, the fifth layer consisted of the same grain size class (250 µm). This lowest layer determines the supply from below. Thus, by assigning the same grain size, large deviations between the cases were prevented that would have occurred if all superimposed sediment was eroded.

3.3. Simulation time and wind forcing

Runs of 10 minutes, 1 day, and 1 year were executed to assess the effect of grain size variations across time scales. The 10-minute runs involved constant wind speeds between 0 and 30 m/s. The 1 day and 1 year academic cases were simulated with varying winds that were created with the wind generator in AeoLiS. The wind generator creates a random wind velocity time series with a given mean and maximum wind speed using a Markov Chain Monte Carlo approach based on a Weibull distribution. A mean wind speed of 10 m/s with a maximum wind speed of 30 m/s was used as input for the wind generator. Generated wind speeds fluctuate on the scale of the model timestep, *dt*, which was varied based on the simulation time (Table 2).

Table 2 – AeoLiS model settings and wind input for scenarios with different temporal scales

Simulation time	***dt***	**Output_times**	**Wind regime**	**# of layers**	**Layer_thickness**
10 minutes	1	10	Constant, range from 0 to 30 m/s	5	0.00005
1 day	60	600	Variable, mean 10 m/s, max 30 m/s	5	0.0001
1 year	3600	86400	Variable, mean 10 m/s, max 30 m/s	5	0.01

The layer thickness used in the simulations (Table 2) was scaled to the time step. This was done to avoid sediment depletion in the surface layer during time steps with peak transport, which would influence calculated transport rates. Increasing the resolution for the longer time scales is possible with a reduced time step. However, this would greatly increase the computation time needed for each simulation. We tested whether increasing the vertical resolution from 5 to 50 layers would have an effect on the 10-minute time scale of the vertical layering scenario with a constant 10 m/s wind. The test showed that the sediment flux remained similar (i.e., a difference < 3%). However, there were some minor differences in the temporal trends of the pickup of the coarse and fine sediment, which were related to (numerical) diffusion of the vertical grain size gradient in the 5 layer test. These effects might be exacerbated at longer time scales and with the inclusion of varying wind speeds in a simulation. Therefore, the quantitative aeolian sediment transport results that were obtained at different time scales for each case, were not directly compared in this paper.

4. Results

4.1. The transport of single-fraction sediment

Distinct variations in the way different grain sizes reacted to varying wind speeds on the 10 minute time scale were observed in the model results (Figure 5a). Below 10 m/s, the threshold for transport was barely exceeded, and little to no sediment flux occurred for grain sizes between 250 and 500 µm. Between 10 and 15 m/s, the differentiation between the grain size cases was the largest. For these wind speeds, the behavior of the shear velocity and threshold shear velocity following Equation 2 and 3 is shown in Figure 5b. As finer grain sizes have a lower threshold velocity (red line in Figure 5a), transport was initiated at lower wind speeds. For wind speeds above 15 m/s, sediment transport occurred in all grain size cases. Because the shear velocity increased with the wind velocity (Equation 2) and the sediment flux is cubically related to the difference between the shear velocity and the threshold shear velocity (Equation 1), the transport that occurred at a 30 m/s wind speed was more than an order of magnitude higher than that at a 15 m/s wind speed.

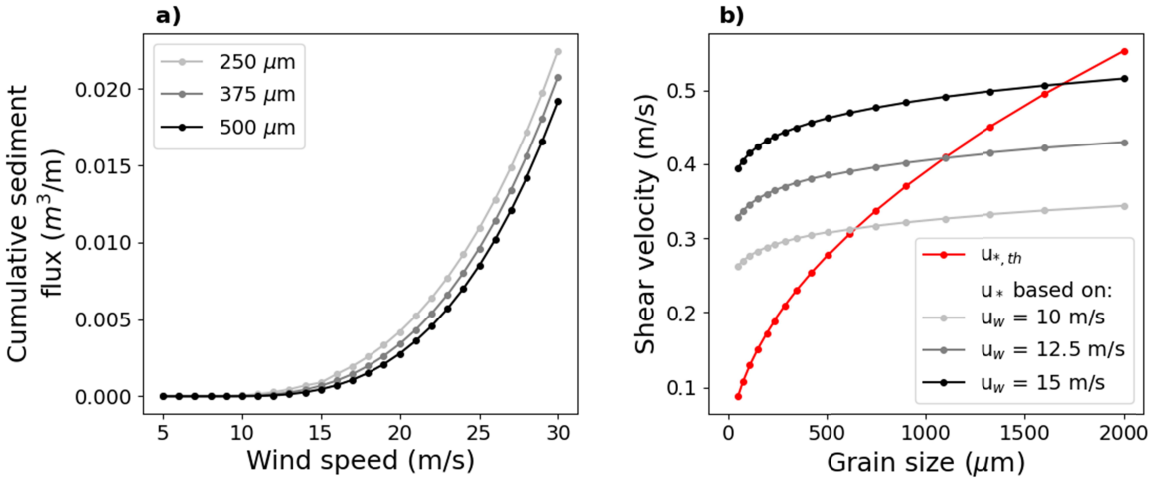

Figure 5 – (a) The cumulative sediment flux after 10 minutes for wind speeds of 0 to 30 m/s for grain sizes of 250, 375 and 500 µm. (b) The relation between grain size and the threshold shear velocity $u_{*,th}$ as follows from Equation 2 in red, and the relation between grain size and the shear velocity u_* for three different wind speeds as follows from Equation 3 (greyscale lines). The shear velocity u_* varies with grain size due to the dependence of the aerodynamic roughness z_0 on the grain size in Equation 3.

On the 1-day time scale, a larger transport magnitude occurred for the 250 and 375 µm cases than the 500 µm case (Figure 6b). The difference in transport between the three cases was largest in the moments with high wind speeds. Throughout time, the difference in the cumulative sediment flux between the grain size cases increased (Figure 6c), which is the result of both the difference in threshold

velocity and the transport magnitude. For finer grain sizes, the lower threshold velocity resulted in a longer time period in which transport could occur, and in that time period, the transport was higher than that for the coarser grain sizes (Figure 6a).

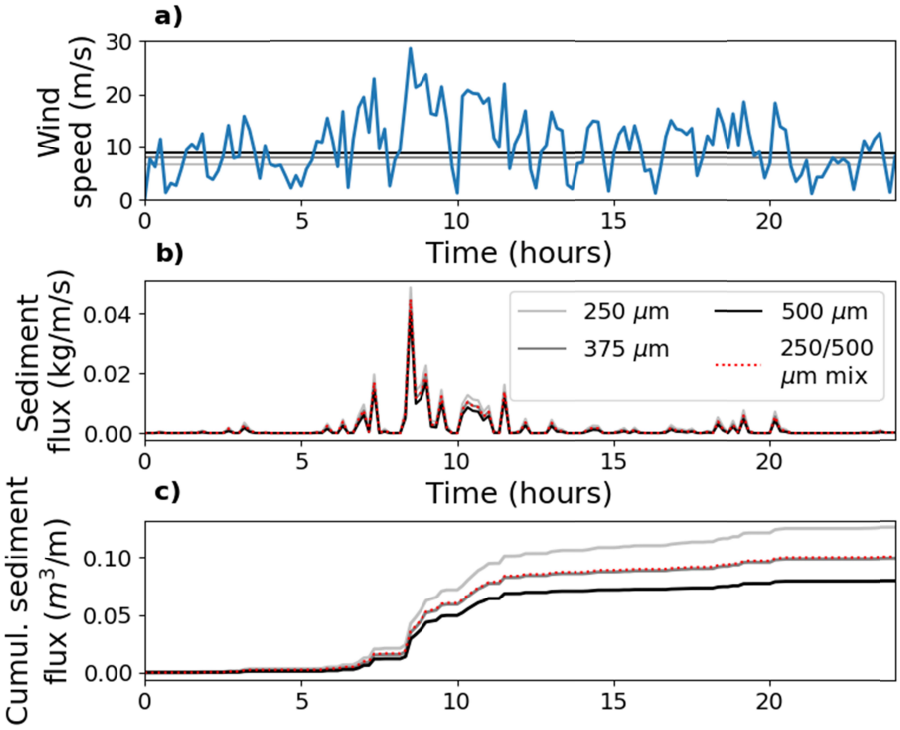

Figure 6 – (a) One-day variable wind scenario which results in the (b) sediment flux and (c) cumulative sediment flux of the single-fraction cases of 250, 375, and 500 µm and of a two-fraction 250/500 µm mix (50-50% mix, Figure 3b). The horizontal lines in the wind plot indicate the threshold velocity for the single-fraction case with the corresponding color in (b) and (c).

4.2. Comparison between single-fraction and two-fraction mixes

The 50-50% mix with the 250 and 500 µm sediment fractions resulted in similar transport rates as the single-fraction simulation with the average grain size of 375 µm (Figure 6c). For the simulated wind climate, there was little effect of the coarsening of the top layer. There was some differentiation between the mix and the 375 µm case in periods where the wind speed was around the threshold velocity of the different fractions. However, the highest wind speeds resulted in the largest contribution to the sediment flux. Thus, the differentiation at lower wind speeds was negligible on the scale of the total cumulative sediment flux during the one-day simulation. For the higher wind speeds, the larger and

smaller transport that occurred for the 250 µm and 500 µm fractions in the mix balanced each other, making the resulting cumulative transport comparable to the 375 µm case. This equalization may occur because the shear velocity and threshold shear velocity in Figure 5b show approximately linear trends for this relatively limited grain size range. At the yearly time scale, the behavior of the two-fraction mix was also closely replicated with a single fraction equal to the average grain size of the mix.

The effect of armoring was further investigated with 80-20% mixes of varying grain sizes (125/2000 µm, 300/1300 µm, and 375/1000 µm) with a constant average grain size equal to 500 µm. At a yearly timescale, the cumulative sediment flux varied for the different mixes (Figure 7). The 375/1000 µm case aligned with the result of the average grain size, the 300/1300 µm mix was slightly larger, and the 125/2000 µm mix showed larger deviations. At the start of the year, the cumulative sediment flux of the 125/2000 µm mix exceeded that of the average grain size. Within the first 50 days, it even exceeded the cumulative sediment flux of the single-fraction 125 µm case. The explaining mechanism is the increase of the aerodynamic roughness in the mix that was caused by the coarse fraction. A larger aerodynamic roughness increases the shear velocity (greyscale lines in Figure 5b) and, thus, the transport capacity which is dependent on the difference between the shear velocity and the threshold shear velocity (Equation 1). After the 50-day period, this increased transport capacity was counteracted by the coarsening of the bed surface (Figure 7), and the cumulative sediment flux progressively got closer to the reference case. After 240 days, the cumulative transport of the 125/2000 µm case became even lower than the reference case, eventually resulting in approximately 15% less cumulative transport at the end of the year. Similar fluctuations in the difference in cumulative sediment flux occurred for the 300/1300 µm mix, although, the cumulative sediment flux was never less than the reference case.

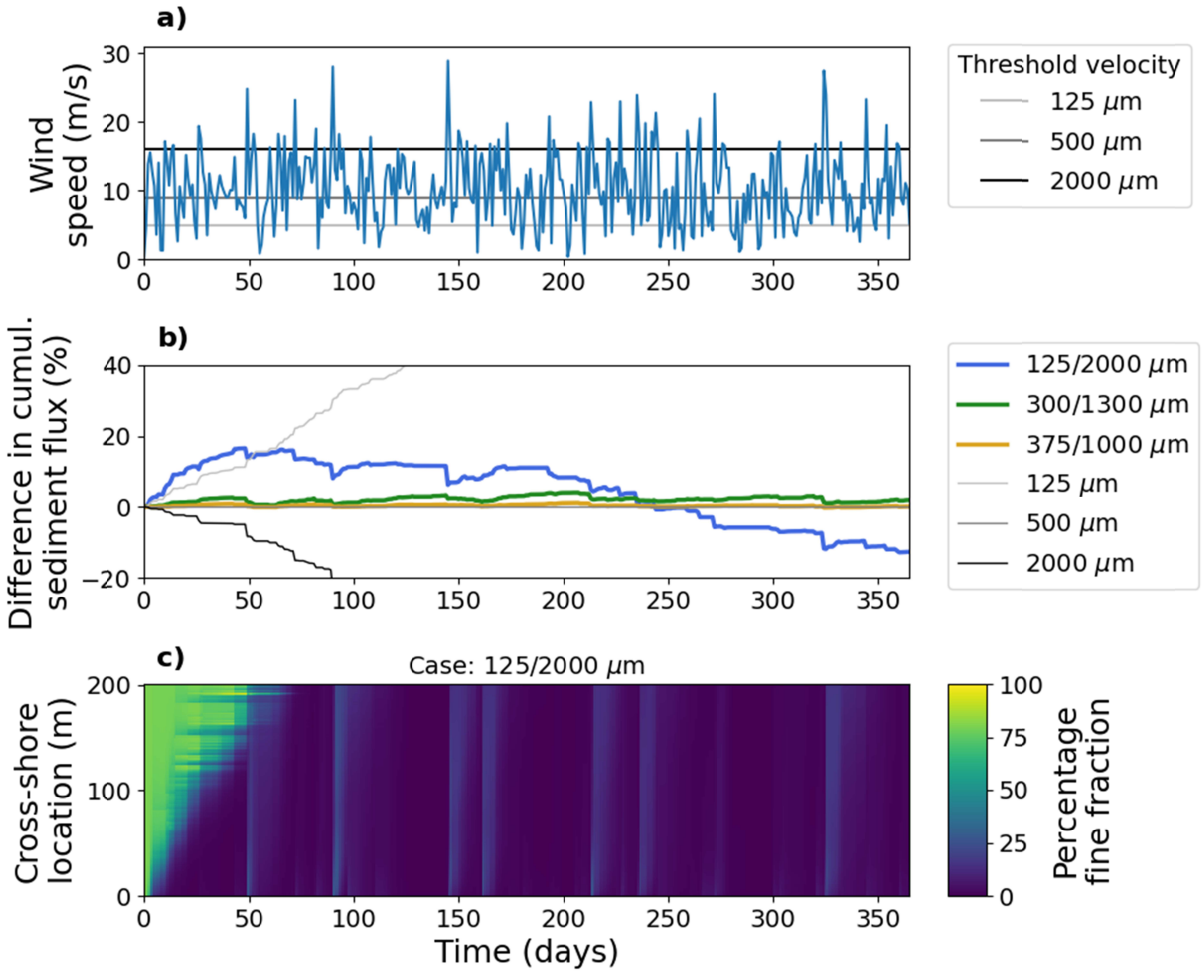

Figure 7 - (a) 1-year variable wind scenario. The horizontal lines in the wind plot indicate the threshold velocity for single-fraction cases with colors corresponding to the sediment fluxes in (b). (b) Cumulative sediment flux of the single-fraction cases of 125 µm (light grey), 500 µm (grey), and 2000 µm (black), compared to the cumulative sediment flux that occurs for the 80-20% mixes (Figure 3c) in blue, green, and yellow that all have an average grain size of 500 µm. Note that the single-fraction case of 500 µm is used as the reference case. (c) Time-stack of the development of the percentage of fine fraction that is present in the top layer of the bed surface for the 125/2000 µm mix through time (x-axis) and space (y-axis).

4.3. The effect of coarse fraction percentage on sediment transport

Not only the size but also the relative percentage of the coarse fraction affects the cumulative sediment flux (Figure 8). The effect of the percentage of coarse fraction was investigated by varying the coarse sediment percentage between 1 and 20% in a 125/2000 µm mix (Figure 3d). The 80-20% case showed a strong deviation in the cumulative sediment flux compared to the reference case (100% 125 µm) resulting in a decrease in the yearly cumulative transport rate of more than 50% (Figure 8b). The

decrease in transport due to armoring occurred from 70 days and onwards. For the 90-10% case, it took 150 days for this deviation to occur, and the deviation after a year was smaller, at approximately 30% less transport than the reference case. The cases where only 1 or 5% of coarse fraction was present did not show a considerable deviation from the sediment flux of the fine fraction within the 1-year time frame. All cases showed how wind speed peaks affect the cumulative sediment flux. The wind speed peaks cause mobilization of the coarse fraction at the bed surface, which exposes finer fractions that are more easily transported (Figure 8c).

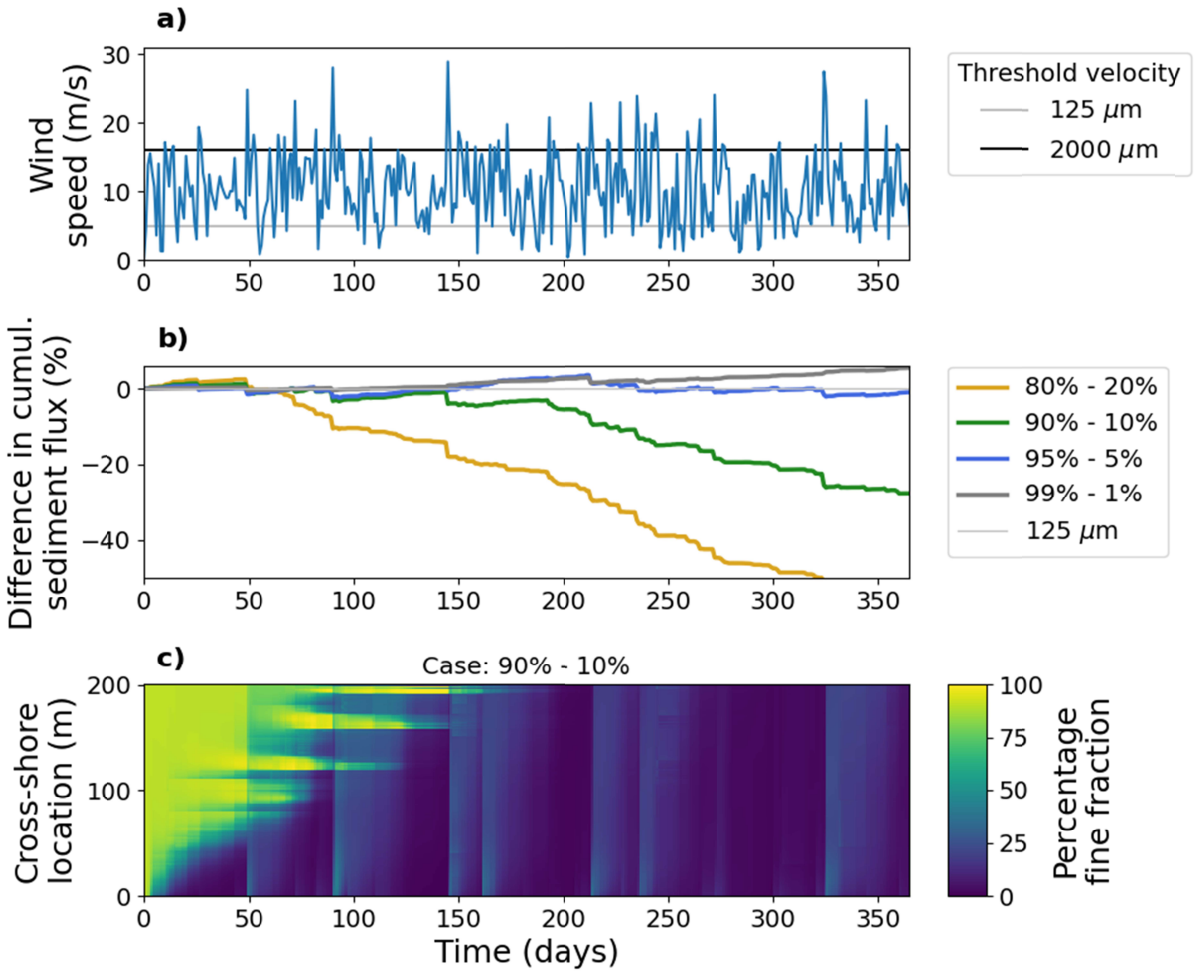

Figure 8 – (a) 1-year variable wind scenario. The horizontal lines in the wind plot indicate the threshold velocity for the single-fraction case of 125 µm (light grey) and 2000 µm (black). (b) Cumulative sediment flux of the reference single-fraction case of 125 µm (light grey), compared to the cumulative sediment flux that occurs for two-fraction mixes in yellow, green, blue, and grey that consist of varying percentages of the 125 and 2000 µm fractions (Figure 3d). (c) Time-stack of the development of the percentage of fine fraction that is present in the top layer of the bed

surface through time (x-axis) and space (y-axis), visualized for the 125/2000 µm mix that starts with 90% fine and 10% coarse fraction.

4.4. The effect of different particle size distributions on sediment transport

Compared to the two fraction mixes, the simulations with full particle size distributions resulted in less deviation from the reference case (median grain size of the PSD). The maximum difference in cumulative sediment flux was 15% and 7.5% less transport after the 1-day (Figure 9) and 1-year period (Figure 10), respectively. Overall, all PSDs showed comparable trajectories, except for PSD 6, which has the widest distribution. In the 1-day period, PSD 6 showed several hours with a larger cumulative sediment flux than the reference grain size. This might have been related to a relatively large aerodynamics roughness and fine fraction abundance, caused by the shape of PSD 6 (Figure 3e). In the 1-year period, PSD 6 remained relatively close to the reference grain size up until day 200, whereas the other PSDs already showed significant deviations near the start of the simulation. Again, this behavior might be caused by the balance between the presence of coarse and fine fractions in the grain size distribution.

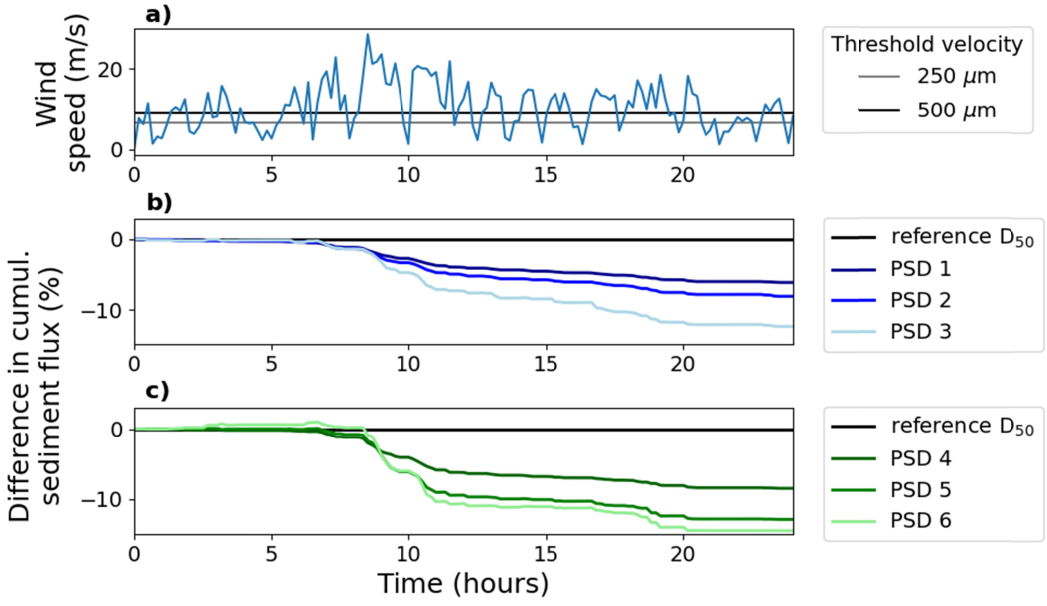

Figure 9 – (a) 1-day variable wind scenario. The horizontal lines in the wind plot indicate the threshold velocity for the single-fraction case of 250 µm (grey) and 500 µm (black). (b) and (c) Cumulative sediment flux of each tested particle size distribution (PSD) as shown in Figure 3e, compared to the reference case (black). For each PSD, the reference case corresponds to the median grain size of the PSD. The blue colors in (b) have a median grain size of around 250 µm, the green colors in (c) have a median grain size around 500 µm.

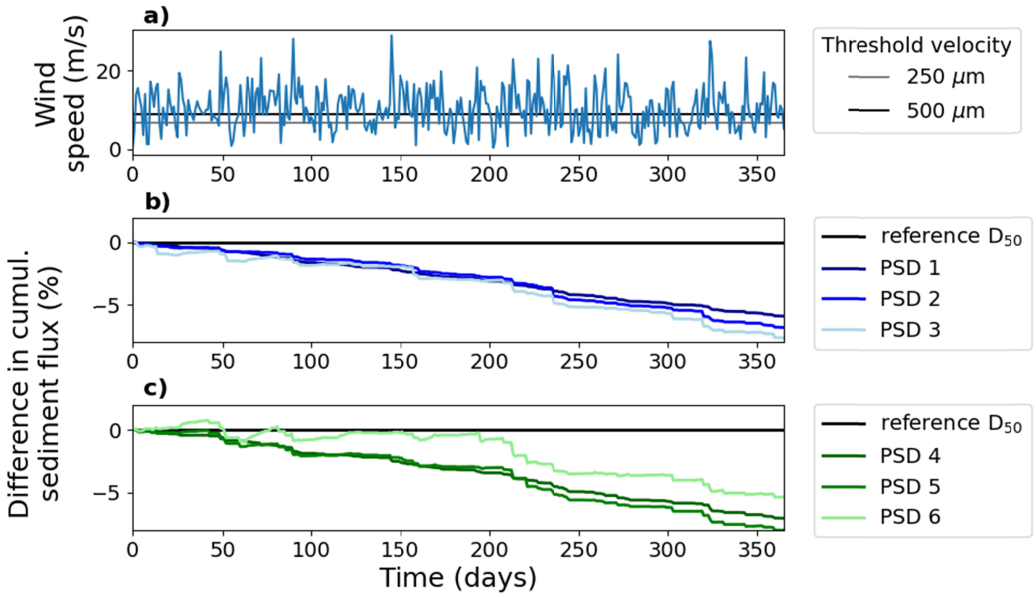

Figure 10 – (a) 1-year variable wind scenario. The horizontal lines in the wind plot indicate the threshold velocity for the single-fraction case of 250 µm (grey) and 500 µm (black). (b) and (c) Cumulative sediment flux of each tested particle size distribution (PSD) as shown in Figure 3e, compared to the reference case (black). For each PSD, the reference case corresponds to the median grain size of the PSD. The blue colors in (b) have a median grain size of around 250 µm, the green colors in (c) have a median grain size around 500 µm.

4.5. The impact of grain size variability in the horizontal dimension

The horizontal variation cases with different spatial gradients showed distinctly different cumulative sediment fluxes when simulated for a 10-minute period with a constant 10 m/s speed. The finer the sediment at the start of the domain, the higher the cumulative sediment flux (Figure 11). In Figure 11b, c, and d, the erosion area in the domain is indicated with white hatching, where leftward leaning hatching indicates pickup of the fine fraction and rightward leaning hatching indicates pickup of the coarse fraction. The variation in the cross-shore expanse of the erosion area between the different scenarios indicates a variation in the fetch length, which could have been caused by a difference in the magnitude of the equilibrium transport. Coarse sediment resulted in a lower equilibrium transport magnitude (Equation 1), so based on the implementation of the adaptation timescale, the distance needed to reach the equilibrium transport was smaller than with fine sediment at the start of the domain which is related to a larger equilibrium transport. The larger bed roughness that occurred for the coarse sediment counteracted this effect slightly. In conclusion, the fetch length is shorter when coarser sediment is present at the start of the domain, and as fully developed transport was reached at

the end of the erosion area, there was no significant impact of the bed surface gain size composition further along the domain.

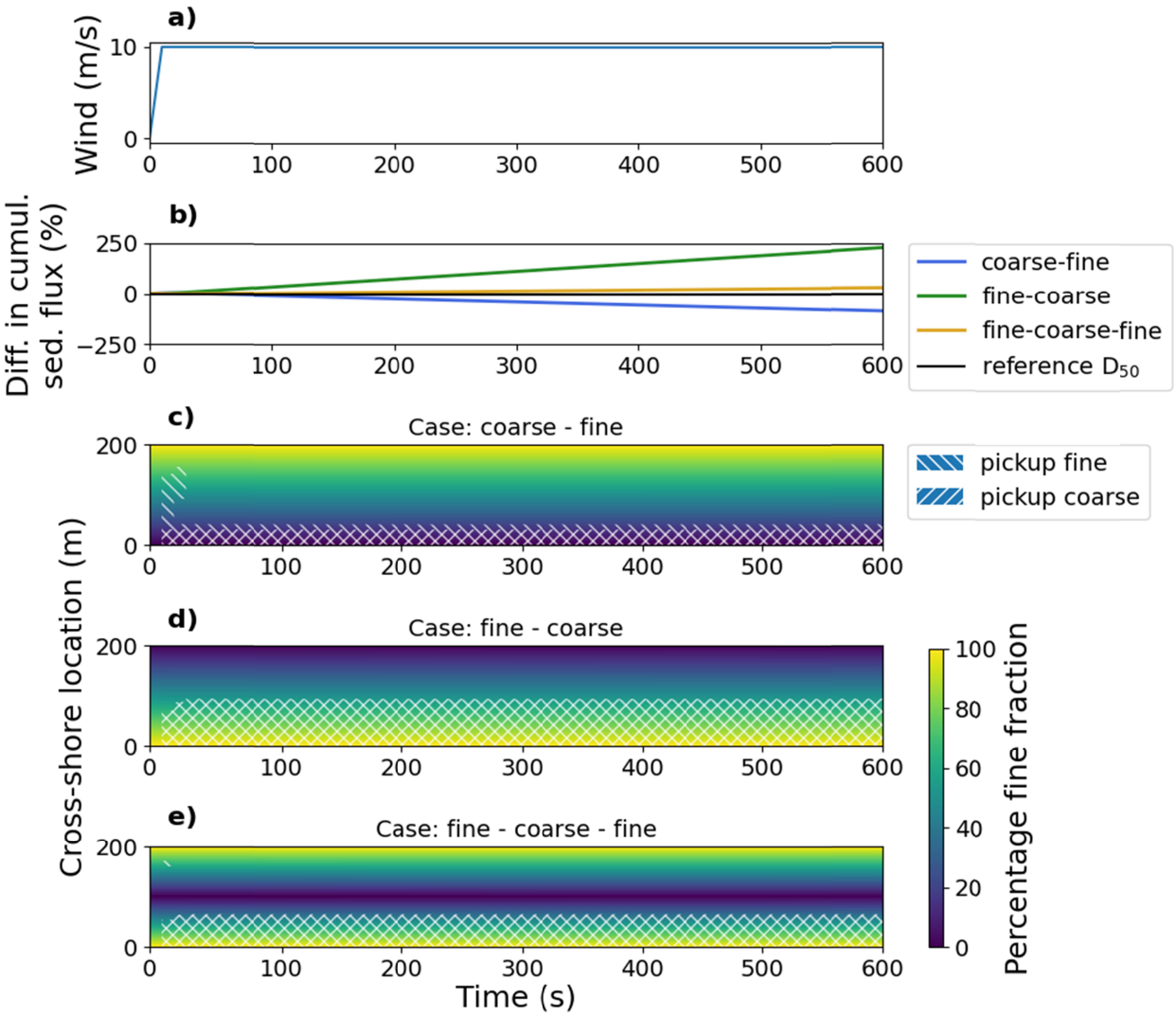

Figure 11 - (a) Cumulative sediment fluxes under a 10-minute, constant 10 m/s wind speed for the horizontal variation scenario (Figure 4a), which includes a coarse to fine (blue), fine to coarse (green) and fine to coarse to fine (yellow) gradient, compared to the reference grain size of 375 µm (black). Time-stack of the development of the percentage of fine fraction that is present in the top layer of the bed surface for the (b) coarse to fine, (c) fine to coarse and (d) fine to coarse to fine case.

The 1-day and 1-year simulations of the horizontal grain size variations resulted in similar sediment flux behavior. The coarse-fine case resulted in less transport than the reference D_{50} and the fine-coarse and fine-coarse-fine cases resulted in more transport (Figure 12). The bed surface layer development of the

coarse-fine case showed coarsening of the surface (Figure 12c), whereas the fine-coarse case showed fining (Figure 12d). For each case, a unique cross-shore equilibrium bed composition developed at the bed surface. The occurrence of pickup throughout the domain seemed most strongly related to the wind speed. However, after the formation of the equilibrium grain size gradient, the region with pickup became much larger for both periods and all cases.

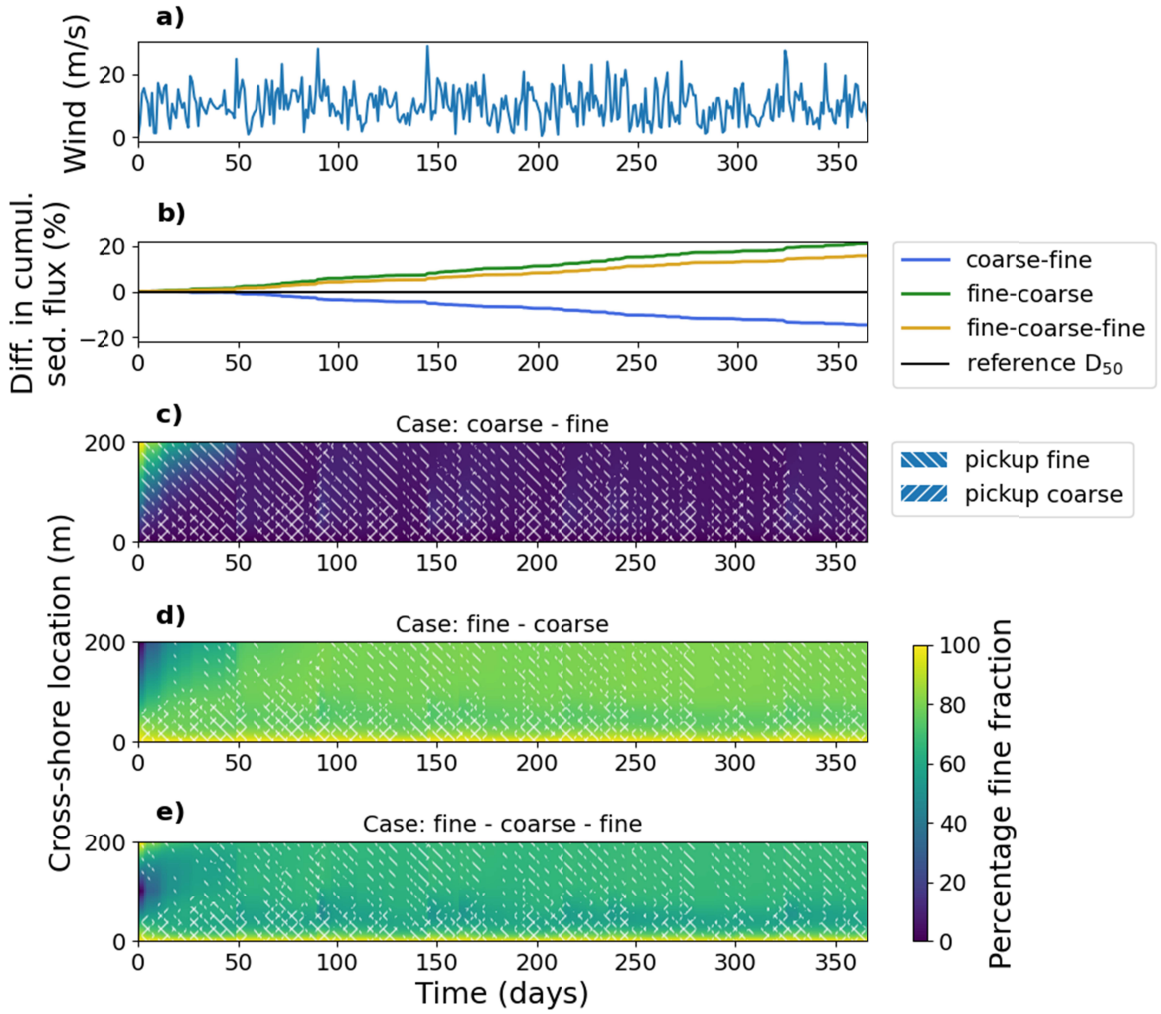

Figure 12 - (a) 1-year variable wind scenario. (b) Cumulative sediment fluxes of the horizontal variation scenario (Figure 4a), which includes a coarse to fine (blue), fine to coarse (green) and fine to coarse to fine (yellow) gradient, compared to the reference grain size of 375 µm (black). Time-stack of the development of the percentage of fine fractions that is present in the top layer of the bed surface for the (b) coarse to fine, (c) fine to coarse and (d) fine to coarse to fine case.

4.6. Sediment transport variations due to vertical grain size variability

The vertical grain size layering directly affected the amount and timing of aeolian transport during the different time scales. For the 10-minute simulations, varying behavior was observed depending on the wind speed and the vertical location of the coarse layer (Figure 13). At a wind speed of 10 m/s, little transport occurred due to the relatively low wind speeds, and the grain size fraction in the upper layer of both cases dominated the cumulative sediment flux (Figure 13a). At 20 m/s, the removal of the coarse and fine fraction for the 1st layer coarse and 4th layer coarse case, respectively, resulted in a reduction of the difference in the cumulative sediment flux compared to the reference grain size (Figure 13b). At 30 m/s, both the fine and coarse sediment were easily mobilized by the wind, resulting in a considerably lower difference in cumulative sediment flux compared to the reference grain size (Figure 13c).

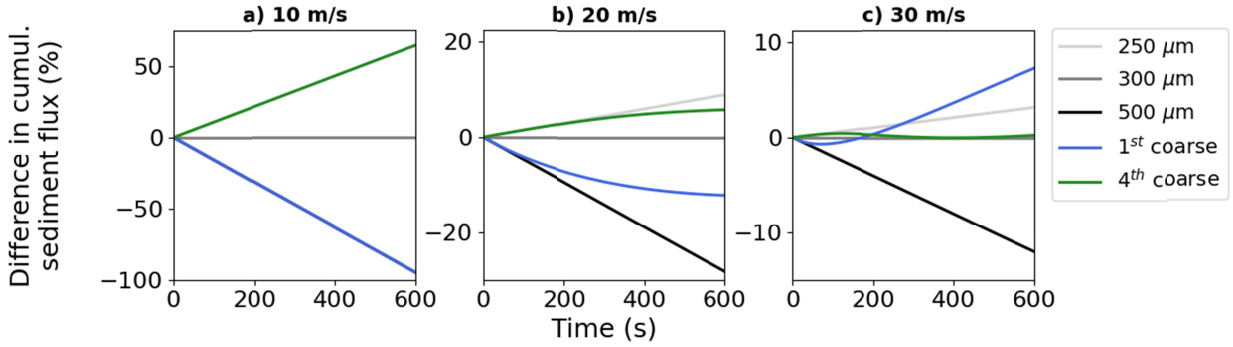

Figure 13 - Cumulative sediment fluxes of the vertical layering scenario (Figure 4b) compared to the reference grain size 300 µm (grey) for 10-minute simulations with a constant wind speed of (a) 10 m/s, (b) 20 m/s, and (c) 30 m/s. The scenario includes the case where the top layer (blue) and the fourth layer (green) consisted of a coarse fraction (500 µm). The other layers consisted of a fine fraction (250 µm). For comparison, the cumulative sediment flux of the single-fraction case of 250 (light grey) and 500 µm (black) are shown.

On the scale of a 1-day simulation, the main differentiation in the cumulative sediment flux between the vertical layering cases and the reference grain size (Figure 14b) occurred during the wind peak between hours 5 and 10 (Figure 14a). This wind peak caused the coarse and fine sediment of, respectively, the 1st coarse case and 4th coarse case to be removed from the surface layer (Figure 14 c and d). Subsequently, a relatively stable spatial grain size gradient formed, and the difference in cumulative sediment flux showed limited change for both cases. As the spatial grain size gradient of the bed surface layer changed, the extent of the pickup area, especially for the coarse fraction, increased. Overall, the 1-year simulation, showed comparable trends to the 1-day simulation, although the difference in cumulative sediment flux compared to the reference was lower (around 1% vs. 5%).

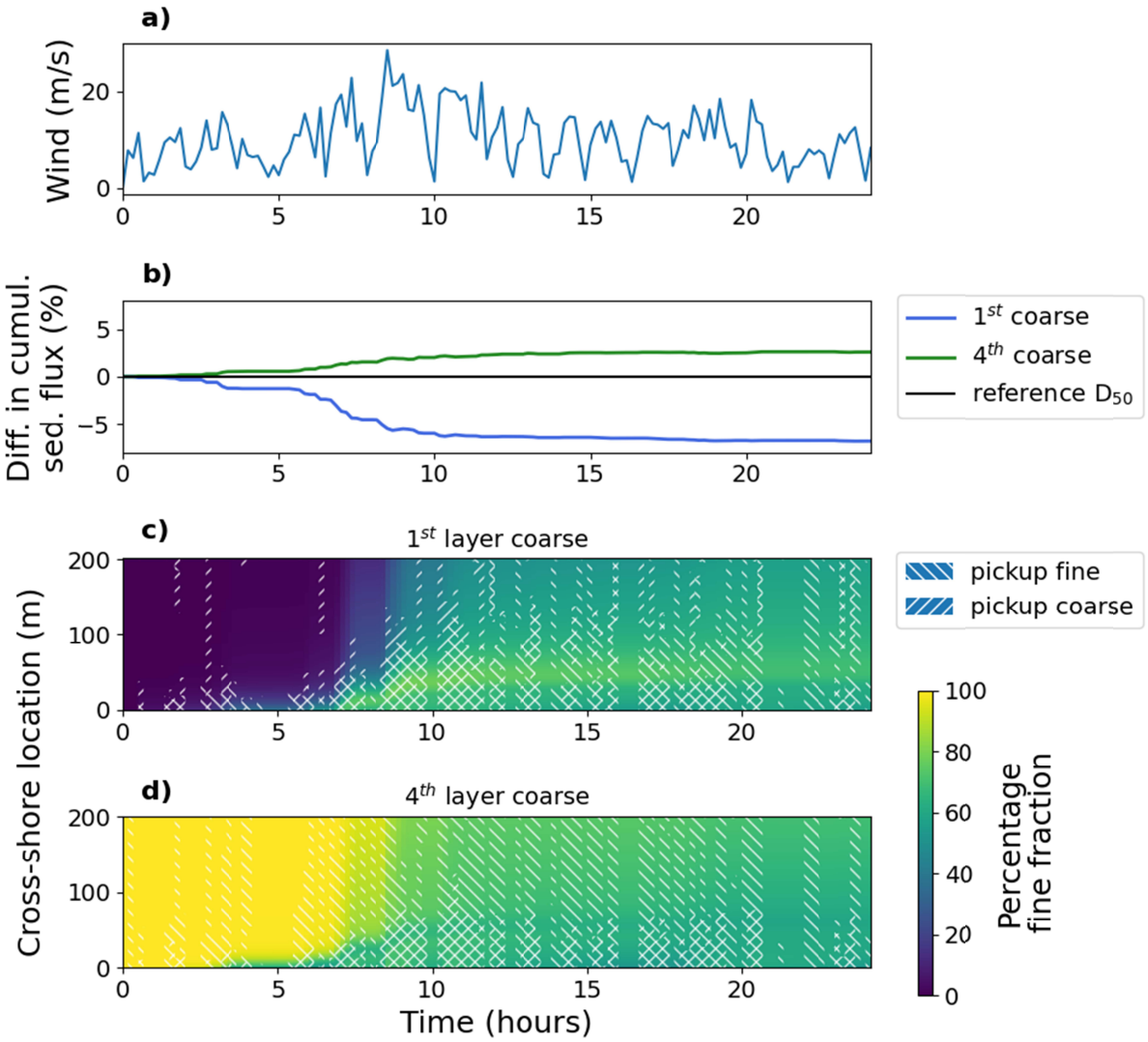

Figure 14 - (a) 1-day variable wind scenario. (b) Cumulative sediment fluxes of the vertical layering scenario (Figure 4b) compared to the reference grain size 300 µm (black). The scenario includes case 1 (blue), where the top layer consisted of a coarse fraction, and case 2 (green), where the fourth layer consisted of a coarse fraction (500 µm). The other layers consisted of a fine fraction (250 µm). Time-stack of the development of the percentage of fine fractions that is present in the top layer of the bed surface for (b) case 1 and (c) case 2.

5. Discussion

5.1. Using a single-fraction representative grain size in aeolian sediment transport modeling

The cumulative sediment flux calculated with multi-fraction transport and its approximation with a single-fraction reference grain size were similar on time scales of days to years. There only was a considerable impact on the yearly cumulative transport when a relatively large content of coarse grains,

480 >10% of 2000 µm sediment, was present. The full PSD scenarios, which are similar to the grain size
481 distribution of beach sand, resulted in a maximum transport reduction of 15% over one day and 7.5%
482 over one year compared to the median grain size. These values are in a similar order of magnitude as
483 those found by Hoonhout & de Vries (2016), although the presence of shells further exacerbated the
484 resulting reduction in their study. The results indicate that for most scenarios, the median grain size can
485 be used as a pragmatic metric for natural grain size distributions in aeolian sediment transport models
486 at daily to yearly time scales.

487 However, there are some limitations to simplifying grain size distributions with the median grain size. In
488 some of the single-fraction simulations, larger transport rates were recorded than in the corresponding
489 multi-fraction simulation. Wide PSDs might include a relatively large contribution of both coarse and fine
490 fractions. The fine fraction abundance may result in a relative increase of total transport compared to
491 narrower PSDs (e.g., PSD 6 compared to PSD 4 and 5 in Figure 10). Additionally, several multi-fraction
492 cases showed that increased transport can occur despite an increase in the reference grain size (e.g., the
493 125/2000 µm mix in Figure 7). This sediment transport increase is related to an increase in the bed
494 roughness and the shear velocity (Equation 3). In all cases, the effect was temporary, as coarsening due
495 to the removal of fines counteracted the increase in transport caused by the roughness.

496 The suitability of the D_{50} as a representative grain size can also be affected by armoring that limits the
497 aeolian sediment transport. These armoring effects occur when a considerable amount of coarse grains
498 is present. Whether specific grain sizes will result in armoring depends on the local wind climate. During
499 energetic wind events, wind peaks can cause an increase in sediment transport and mobilization of
500 coarse grains from the bed surface, which can expose underlying sediment (e.g., the 125/2000 µm mix
501 in Figure 7). For the synthetic wind climate that was generated and used in this study, about 2000 µm
502 was a critical grain size. Future work could further quantify for which wind climates and grain size
503 distributions the use of the D_{50} as a representative grain size is valid. For now, a representative wind
504 forcing could be created based on the wind climate and used in an aeolian sediment transport model to
505 determine to what extent specific coarse fractions are expected to be mobilized.

506 Besides wind speed peaks, hydrodynamic processes and trampling can also break up and alter armor
507 layers. Hydrodynamic processes can cause erosion, deposition and mixing that directly affect the top
508 layers of the bed surface on a time scale of seasons (e.g., Abuodha, 2003; Prodger et al., 2017), events
509 (e.g., Gallagher et al., 2016) and tides (e.g., van IJzendoorn et al., 2022). Future work could investigate
510 the effect of temporally varying grain sizes due to hydrodynamic processes on the sediment flux by

511 including temporal grain size variations in modeling simulations by making simplified assumptions (e.g.
512 based on findings by van IJzendoorn et al., 2022) or coupling with a numerical model (Reniers et al.,
513 2013; Srisuwan & Work, 2015). Trampling is also expected to affect the grain size at the bed surface
514 (Moayeri et al., 2023; Reyes-Martínez et al., 2015). Its effects could be included in aeolian sediment
515 transport models with mixing of surface layers in locations where human activity is expected.

516 **5.2. The implementation of spatial grain size variations in aeolian sediment transport modeling**

517 Significant vertical grain size variations at the bed surface have been measured (e.g., van IJzendoorn et
518 al., 2022) and over larger soil depths (e.g., Gallagher et al., 2016; Gunaratna et al., 2019). The
519 measurements of van IJzendoorn et al. (2022) showed a maximum range of 119 µm in the D_{50} of
520 different layers in the top 5 cm of the bed surface. Based on our results, we expect that these variations
521 could be simulated relatively accurately on the daily and yearly timescales with the D_{50}. On the minute-
522 scale, we expect that the sediment flux could significantly be altered, especially when layers with a
523 significant contribution of coarse fraction are present near the bed surface. We recommend the
524 inclusion of vertical grain size layering in aeolian sediment transport models where short-term time
525 scales are considered. On time scales longer than days, they can be omitted.

526 The source area at the beginning of the domain has a significant impact on the cumulative sediment flux
527 across all time scales. As a result, there can be a disconnect between the grain size that is at the bed
528 surface and the transport that occurs at that location. Consider a point measurement at the end of the
529 domain of the coarse - fine and fine - coarse - fine cases for the 10-minute time scale (Figure 13). The
530 grain size at these locations was comparable but the cumulative sediment flux deviated considerably.
531 This difference was mostly related to the grain size of the material present in the source area where
532 pickup of fine and coarse sediment occurred. This shows it is important to consider the grain size that is
533 present in the source area when explaining minute-scale sediment transport measurements, as
534 previously indicated by Cohn et al., (2022), Field and Pelletier (2018) and Uphues et al. (2021). These
535 grain size measurements should be recent because wind speed peaks can cause temporal variations in
536 the bed surface grain size and the related aeolian sediment transport.

537 The intertidal area was found to be an important source for aeolian sediment transport towards the
538 dunes by de Vries, (2014a). Our findings show that this upwind source of sediment is important for the
539 bed surface grain size development across the domain and the sediment transport magnitude. Thus, the
540 results suggest that the grain size in the intertidal area (e.g., Bascom, 1951) might be the most

important to include in aeolian sediment transport models that are used for coastal dune development predictions. These findings align with measurements of aeolian sediment transport in the intertidal area by Swann et al., (2021), who found similar grain sizes in the air column as on the bed. Future work could further validate or falsify these findings by combining minute-scale quantitative sediment transport measurements with bed surface grain size measurements that can show a temporal variation through time. Furthermore, the importance of the grain size in the intertidal area emphasizes the need to study sediment supply by hydrodynamic processes and, specifically, its effect on grain size composition.

6. Conclusions

The sorting of multi-fraction sediment, spatial variations in grain size, and their impact on aeolian sediment transport were studied using a numerical aeolian sediment transport model. Results show that, in general, the D_{50} can be used as a representative grain size in aeolian sediment transport modeling on a time scale of days to years. For wide grain size distributions, the multi-fraction sediment flux may differ from the single-fraction flux of the reference grain size. In these cases, simplified model runs that include the full particle size distribution and a wind forcing representative for the wind climate to test the impact on the sediment flux could be considered.

On a time scale of 10-minutes, the bed surface grain size has a direct effect on the aeolian sediment transport flux. Due to this strong relation between grain size and sediment transport, vertical grain size layering may be required in models that predict aeolian sediment transport at this time scale. On time scales from days to years, modeling the effect of vertical layering may not be needed if a representative grain size is used.

The effect of horizontal grain size variations is relevant across all time scales. The grain size in the upwind part of the domain can directly affect the transport magnitude across the domain. The intertidal area can be the dominant source of aeolian sediment transport that affects coastal dune development. In these cases, we recommend to include the grain size present in this region in aeolian sediment transport models and consider its impact on point measurements of sediment transport recorded on the beach. Additionally, we recommend to further investigate the supply of sediment to the intertidal zone by marine processes, specifically focusing on grain size.

Acknowledgments

This work is part of the research program DuneForce with project number 17064, which is (partly) financed by the Dutch Research Council (NWO)

Data availability statement

Version 2.1.0 of the AeoLiS software used for the aeolian sediment transport simulations in this research is preserved at https://doi.org/10.4121/22215562, available via GPL-3.0 and developed openly on Github (https://github.com/openearth/aeolis-python). The Python code used for the analysis and figure generation is hosted at Github (https://github.com/christavanijzendoorn/grainsizeanalysis-aeolis) and is preserved at https://doi.org/10.4121/22220134, version 1.1.0, under GPL-3.0.

References

Abuodha, J. O. Z. (2003). Grain size distribution and composition of modern dune and beach sediments, Malindi Bay coast, Kenya. *Journal of African Earth Sciences*, *36*(1–2), 41–54. https://doi.org/10.1016/S0899-5362(03)00016-2

AeoLiS Development Team. (2023). *AeoLiS (Version v2.1.0). [Software]*. 4TU Repository. https://doi.org/10.4121/22215562

Anderson, R. S., & Haff, P. K. (1988). Simulation of Eolian Saltation. *Science*, *241*(4867), 820–823. https://doi.org/10.1126/SCIENCE.241.4867.820

Bagnold, R. A. (1937a). The size-grading of sand by wind. *Proceedings of the Royal Society of London. Series A - Mathematical and Physical Sciences*, *163*(913), 250–264. https://doi.org/10.1098/rspa.1937.0225

Bagnold, R. A. (1937b). The Transport of Sand by Wind. *The Geographical Journal*, *89*(5), 409. https://doi.org/10.2307/1786411

Bascom, W. N. (1951). The relationship between sand size and beach-face slope. *Eos, Transactions American Geophysical Union*, *32*(6), 866–874. https://doi.org/10.1029/TR032I006P00866

Bauer, B. O. (1991). Aeolian Decoupling of Beach Sediments. *Annals of the Association of American Geographers*, *81*(2), 290–303. https://doi.org/10.1111/j.1467-8306.1991.tb01691.x

Bauer, B. O., & Davidson-Arnott, R. G. D. (2002). A general framework for modeling sediment supply to coastal dunes including wind angle, beach geometry, and fetch effects. *Geomorphology*, *49*(1–2), 89–108. https://doi.org/10.1016/S0169-555X(02)00165-4

Bristow, N. R., Best, J., Wiggs, G. F. S., Nield, J. M., Baddock, M. C., Delorme, P., & Christensen, K. T. (2022). Topographic perturbation of turbulent boundary layers by low-angle, early-stage aeolian

599 dunes. *Earth Surface Processes and Landforms*, *47*(6), 1439–1454.
600 https://doi.org/10.1002/ESP.5326

601 Çelikoğlu, Y., Yüksel, Y., & Sedat Kabdaşli, M. (2006). Cross-Shore Sorting on a Beach under Wave Action.
602 *Journal of Coastal Research*, *22*(3 (223)), 487–501. https://doi.org/10.2112/05-0567.1

603 Cheng, H., He, J., Zou, X., Li, J., Liu, C., Liu, B., … Kang, L. (2015). Characteristics of particle size for
604 creeping and saltating sand grains in aeolian transport. *Sedimentology*, *62*(5), 1497–1511.
605 https://doi.org/10.1111/SED.12191

606 Cohn, N., Dickhudt, P., & Marshall, J. (2022). In-situ measurement of grain size characteristics within the
607 aeolian saltation layer on a coastal beach. *Earth Surface Processes and Landforms*, *47*(9), 2230–
608 2244. https://doi.org/10.1002/ESP.5373

609 de Vries, S., Arens, S. M., de Schipper, M. A., & Ranasinghe, R. (2014a). Aeolian sediment transport on a
610 beach with a varying sediment supply. *Aeolian Research*.
611 https://doi.org/10.1016/j.aeolia.2014.08.001

612 de Vries, S., van Thiel de Vries, J. S. M., van Rijn, L. C., Arens, S. M., & Ranasinghe, R. (2014b). Aeolian
613 sediment transport in supply limited situations. *Aeolian Research*, *12*, 75–85.
614 https://doi.org/10.1016/j.aeolia.2013.11.005

615 Delgado-Fernandez, I. (2010). A review of the application of the fetch effect to modelling sand supply to
616 coastal foredunes. *Aeolian Research*, *2*(2–3), 61–70. https://doi.org/10.1016/j.aeolia.2010.04.001

617 Dong, Z., Wang, H., Liu, X., & Wang, X. (2004). A wind tunnel investigation of the influences of fetch
618 length on the flux profile of a sand cloud blowing over a gravel surface. *Earth Surf. Process.*
619 *Landforms*, *29*, 1613–1626. https://doi.org/10.1002/esp.1116

620 Durán, O., Claudin, P., & Andreotti, B. (2011). On aeolian transport: Grain-scale interactions, dynamical
621 mechanisms and scaling laws. *Aeolian Research*, *3*(3), 243–270.
622 https://doi.org/10.1016/J.AEOLIA.2011.07.006

623 Edwards, A. C. (2001). Grain size and sorting in modern beach sands. *Journal of Coastal Research*, *17*(1).

624 Field, J. P., & Pelletier, J. D. (2018). Controls on the aerodynamic roughness length and the grain-size
625 dependence of aeolian sediment transport. *Earth Surface Processes and Landforms*, *43*(12), 2616–
626 2626. https://doi.org/10.1002/ESP.4420

Gallagher, E. L., Wadman, H., McNinch, J., Reniers, A., & Koktas, M. (2016). A Conceptual Model for Spatial Grain Size Variability on the Surface of and within Beaches. *Journal of Marine Science and Engineering 2016, Vol. 4, Page 38*, *4*(2), 38. https://doi.org/10.3390/JMSE4020038

Gao, X., Narteau, C., & Rozier, O. (2016). Controls on and effects of armoring and vertical sorting in aeolian dune fields: A numerical simulation study. *Geophysical Research Letters*, *43*(6), 2614–2622. https://doi.org/10.1002/2016GL068416

Gillette, D. A., Herbert, G., Stockton, P. H., & Owen, P. R. (1996). Causes of the fetch effect in wind erosion. *Earth Surface Processes and Landforms*, *21*, 641–659. https://doi.org/10.1002/(SICI)1096-9837(199607)21:7

Gunaratna, T., Suzuki, T., & Yanagishima, S. (2019). Cross-shore grain size and sorting patterns for the bed profile variation at a dissipative beach: Hasaki Coast, Japan. *Marine Geology*, *407*, 111–120. https://doi.org/10.1016/J.MARGEO.2018.10.008

Hallin, C., Almström, B., Larson, M., & Hanson, H. (2019a). Longshore Transport Variability of Beach Face Grain Size: Implications for Dune Evolution. *Journal of Coastal Research*, *35*(4), 751–764. https://doi.org/10.2112/JCOASTRES-D-18-00153.1

Hallin, C., Huisman, B. J. A., Larson, M., Walstra, D. J. R., & Hanson, H. (2019b). Impact of sediment supply on decadal-scale dune evolution — Analysis and modelling of the Kennemer dunes in the Netherlands. *Geomorphology*, *337*, 94–110. https://doi.org/10.1016/j.geomorph.2019.04.003

Hallin, C., Larson, M., & Hanson, H. (2019c). Simulating beach and dune evolution at decadal to centennial scale under rising sea levels. *PLOS ONE*, *14*(4), e0215651. https://doi.org/10.1371/journal.pone.0215651

Hoonhout, B., & de Vries, S. (2016). A process-based model for aeolian sediment transport and spatiotemporal varying sediment availability. *Journal of Geophysical Research: Earth Surface*, *121*(8), 1555–1575. https://doi.org/10.1002/2015JF003692

Hoonhout, B., & de Vries, S. (2019). Simulating spatiotemporal aeolian sediment supply at a mega nourishment. *Coastal Engineering*, *145*, 21–35. https://doi.org/10.1016/j.coastaleng.2018.12.007

Houser, C. (2009). Synchronization of transport and supply in beach-dune interaction. *Progress in Physical Geography*, *33*(6), 733–746. https://doi.org/10.1177/0309133309350120

Kroon, A., de Schipper, M., de Vries, S., & Aarninkhof, S. (2022). Subaqueous and Subaerial Beach Changes after Implementation of a Mega Nourishment in Front of a Sea Dike. *Journal of Marine Science and Engineering 2022, Vol. 10, Page 1152*, *10*(8), 1152. https://doi.org/10.3390/JMSE10081152

Krumbein, W. C. (1934). Size frequency distributions of sediments. *Journal of Sedimentary Research*, *4*(2), 65–77. https://doi.org/10.1306/D4268EB9-2B26-11D7-8648000102C1865D

Liu, Y., Liu, X., & Sun, Y. (2021). QGrain: An open-source and easy-to-use software for the comprehensive analysis of grain size distributions. *Sedimentary Geology*, *423*, 105980. https://doi.org/10.1016/J.SEDGEO.2021.105980

McKenna Neuman, C., & Bédard, O. (2017). A wind tunnel investigation of particle segregation, ripple formation and armouring within sand beds of systematically varied texture. *Earth Surface Processes and Landforms*, *42*(5), 749–762. https://doi.org/10.1002/ESP.4019

McKenna Neuman, C., Li, B., & Nash, D. (2012). Micro-topographic analysis of shell pavements formed by aeolian transport in a wind tunnel simulation. *Journal of Geophysical Research: Earth Surface*, *117*(F4), 4003. https://doi.org/10.1029/2012JF002381

Moayeri, V., Miri, A., Shahriari, A., Rahdari, V., & Gill, T. E. (2023). A field study of the surface disturbance effects of animals and motor vehicles on aeolian sediment emission from a silty playa surface. *Environmental Research*, *216*, 114606. https://doi.org/10.1016/J.ENVRES.2022.114606

Owen, P. R. (1964). Saltation of uniform grains in air. *Journal of Fluid Mechanics*, *20*(2), 225–242. https://doi.org/10.1017/S0022112064001173

Prodger, S., Russell, P., & Davidson, M. (2017). Grain-size distributions on high-energy sandy beaches and their relation to wave dissipation. *Sedimentology*, *64*(5), 1289–1302. https://doi.org/10.1111/sed.12353

Reniers, A. J. H. M., Gallagher, E. L., MacMahan, J. H., Brown, J. A., van Rooijen, A. A., van Thiel de Vries, J. S. M., & van Prooijen, B. C. (2013). Observations and modeling of steep-beach grain-size variability. *Journal of Geophysical Research: Oceans*, *118*(2), 577–591. https://doi.org/10.1029/2012JC008073

Reyes-Martínez, M. J., Ruíz-Delgado, M. C., Sánchez-Moyano, J. E., & García-García, F. J. (2015).

Response of intertidal sandy-beach macrofauna to human trampling: An urban vs. natural beach system approach. *Marine Environmental Research*, *103*, 36–45. https://doi.org/10.1016/J.MARENVRES.2014.11.005

Sarre, R. D. (1987). Aeolian sand transport. *Progress in Physical Geography*, *11*(2), 157–182. https://doi.org/10.1177/030913338701100201/ASSET/030913338701100201.FP.PNG_V03

Sherman, D. J. (1992). An equilibrium relationship for shear velocity and apparent roughness length in aeolian saltation. *Geomorphology*, *5*, 419–431.

Sonu, C. J. (1972). Bimodal Composition and Cyclic Characteristics of Beach Sediment in Continuously Changing Profiles. *SEPM Journal of Sedimentary Research*, *42*(4), 852–857. https://doi.org/10.1306/74d72653-2b21-11d7-8648000102c1865d

Srisuwan, C., & Work, P. A. (2015). Beach Profile Model with Size-Selective Sediment Transport. II: Numerical Modeling. *Journal of Waterway, Port, Coastal, and Ocean Engineering*, *141*(2), 04014033. https://doi.org/10.1061/(ASCE)WW.1943-5460.0000274

Stauble, D. K., & Cialone, M. A. (1997). Sediment Dynamics and Profile Interactions: DUCK94. *Proceedings of the Coastal Engineering Conference*, *4*, 3921–3934. https://doi.org/10.1061/9780784402429.303

Swann, C., Lee, D., Trimble, S., & Key, C. (2021). Aeolian sand transport over a wet, sandy beach. *Aeolian Research*, *51*, 100712. https://doi.org/10.1016/J.AEOLIA.2021.100712

van der Wal, D. (2000a). Grain-size-selective aeolian sand transport on a nourished beach. *Journal of Coastal Research*, *16*(3).

van der Wal, D. (2000b). Modelling aeolian sand transport and morphological development in two beach nourishment areas. *Earth Surface Processes and Landforms*, *25*(1), 77–92. https://doi.org/10.1002/(SICI)1096-9837(200001)25:1<77::AID-ESP49>3.0.CO;2-M

van IJzendoorn, C. O. (2023). *Python code for the analysis of AeoLiS grain size scenarios (Version 1.1.0) [Software]*. 4TU Repository. https://doi.org/10.4121/22220134

van IJzendoorn, C. O., Hallin, C., Cohn, N., Reniers, A. J. H. M., & de Vries, S. (2022). Novel sediment sampling method provides new insights into vertical grain size variability due to marine and aeolian beach processes. *Earth Surface Processes and Landforms*. https://doi.org/10.1002/ESP.5518

van Rijn, L. C., & Strypsteen, G. (2020). A fully predictive model for aeolian sand transport. *Coastal Engineering*, *156*, 103600. https://doi.org/10.1016/J.COASTALENG.2019.103600

Zhang, P., Sherman, D. J., & Li, B. (2021). Aeolian creep transport: A review. *Aeolian Research*, *51*, 100711. https://doi.org/10.1016/J.AEOLIA.2021.100711